ACS APPLIED MATERIALS & INTERFACES

www.acsami.org

Research Article

Nanomechanical Filler Functionality Enables Ultralow Wear Polytetrafluoroethylene Composites

Mark A. Sidebottom, Tomas F. Babuska, Sifat Ullah, Nathan Heckman, Brad L. Boyce, and Brandon A. Krick*

Cite This: *ACS Appl. Mater. Interfaces* 2022, 14, 54293−54303

Read Online

ACCESS | Metrics & More | Article Recommendations

ABSTRACT: Surprisingly, certain α-phase alumina filler particles at one to five weight percent can reduce the wear rate of polytetrafluoroethylene (PTFE) by 10,000 times, while other, seemingly comparable α-phase alumina particles provide only modest—by PTFE composite standards—100 times improvements. Detailed studies reveal that size, porosity, and composition of the particles play important roles, but a quantitative metric to support this mechanism is yet to be developed. We discovered the mechanistic importance of friability of the particles, for example, the ability of the particles to fragment at the sliding interface. This work establishes the importance of functionally friable metal-oxide filler particles in creating ultralow wear PTFE−metal-oxide composite systems. We used in situ nanoindentation/electron microscopy experiments to characterize the fracturability of candidate filler particles. A mechanistic framework relating apparent particle fracture toughness and wear is established, where porous low-apparent fracture toughness particles were observed to promote ultralow wear by breaking up during sliding and forming a thin, robust tribofilm, while dense, high-apparent fracture toughness particles abrade the countersurface, limiting the formation of ultralow wear promoting tribofilms. This framework enables use of a new metric to select filler particles for multifunctional, ultralow wear PTFE composites without relying solely on empirical tribological tests of polymer composite materials.

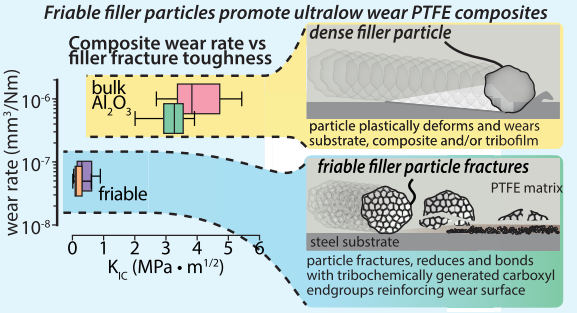

KEYWORDS: *ultralow wear, PTFE, alumina, nanoindentation, tribofilm, fracture toughness, tribochemistry*

1. INTRODUCTION

Polytetrafluoroethylene (PTFE) is a ubiquitous material in sliding interfaces because of its low coefficient of friction ($\mu \sim 0.05-0.2$), high melting temperature (327 °C), and chemical stability.[1−3] The primary limitation of PTFE as a tribological material is that it has a high wear rate ($K \sim 10^{-4}$ to 10^{-3} mm^3/Nm),[4−7] resulting from a delamination wear mechanism caused by cracks propagating through low shear-strength internal interfaces between lamellar crystallites within the PTFE microstructure.[4,8] To mitigate the delamination wear mode of PTFE, different filler particles (ZnO, lead oxides), platelets (MoS_2), and fibers (carbon and glass) have been added to PTFE[4,6,7,9,10] imparting 10−10,000× improvements in wear rate over that of unfilled PTFE. This variability in the wear rate of PTFE composites is a result of the filler particle's ability to act as a multifunctional material that can shut down delamination wear by preventing sub-surface crack propagation,[4,11] supporting normal load along asperities at the sliding interface,[9,12] and promoting transfer film formation.[13−15] While sufficient improvements in the wear rate can be achieved by satisfying one of the above mechanisms, ultralow wear filler materials must meet all requirements.

A special class of PTFE composites containing certain α-Al_2O_3 filler particles show 3 to 4 orders of magnitude improvement in wear performance ($K \sim 3$ to 50×10^{-8} mm^3/Nm) when compared to unfilled PTFE ($K \sim 10^{-4}$ to 10^{-3} mm^3/Nm) under similar sliding conditions.[16−19] This improvement in wear rate is attributed to the formation of ultralow wear surface films (called tribofilms) caused by the shear-induced chain scission of PTFE backbones breaking C−C bonds (i.e., tribochemistry) which react with oxygen and water vapor in the environment to form carboxylic acid end groups. These carboxylic acid end groups chelate to nearby metallic groups, within the steel counterface and alumina particles at the surface of the composite, forming carboxylate metal salts.[20,21] Accumulation of these tribochemical species at the sliding interface creates robust well-adhered tribofilms on

Received: July 29, 2022
Accepted: October 24, 2022
Published: November 23, 2022

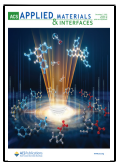

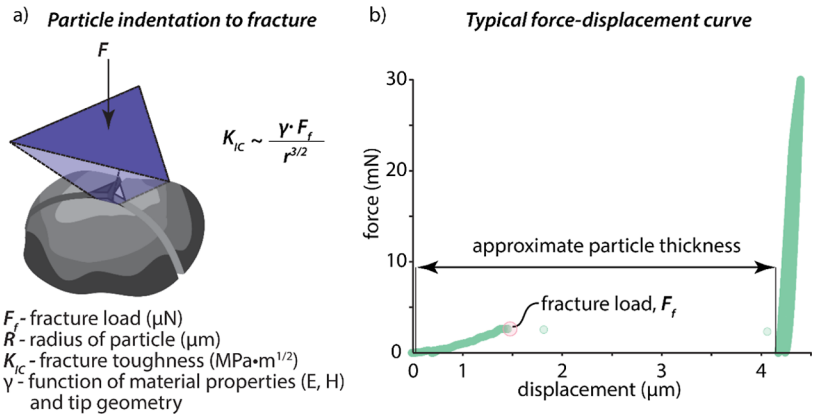

Figure 1. In situ nanoindentation and apparent fracture toughness calculations. (a) Apparent fracture toughness is calculated using fracture load and particle radius. (b) Characteristic force−displacement curve: fracture load and particle thickness may be determined from the force−displacement curve.

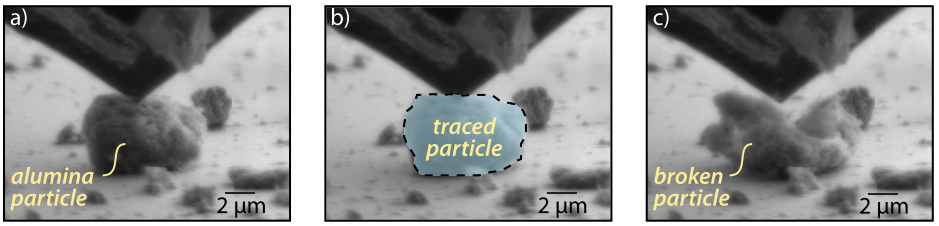

Figure 2. Representative SEM from in situ nanoindentation of alumina particles. (a) Micrograph of the particle before indentation begins. (b) The projected area of the particle is traced. (c) Micrograph of the broken particle after completion of indentation.

both the worn polymer surface and metal counterbody material. These tribochemical species help improve the mechanical properties of the PTFE composite surface[22,23] and help form a protective film (i.e., transfer film) over the counterbody that prevents abrasion.[24,25] 5 wt % α-Al_2O_3 is a common loading fraction for PTFE−α-Al_2O_3 composites though lower weight fractions (as low as 0.1 wt %) have also exhibited low wear rates.[26]

While PTFE−α-Al_2O_3 composites are low wear, not all α-Al_2O_3 filler particles can achieve ultralow wear rates. The promotion of tribochemical species is a single aspect to consider, yet other determining characteristics of the α-Al_2O_3 particles play an important role. Krick et al. evaluated the effect of particle size by testing sets of PTFE−α-Al_2O_3 composites with different particle sizes.[23] Krick et al. measured the diameter and specific surface area of all the different alumina particles composited with PTFE and determined that many particles initially believed to be nanometer in size were actually large micron-sized nanostructured (highly porous) microparticles. The micrometer-scale porous particles were found to be less abrasive than fully dense particles and allowed for the formation of protective tribofilms on both the PTFE composite and metal counterface. Transmission electron microscopy (TEM) and X-ray microtomography of the worn PTFE−α-Al_2O_3 surface revealed that the porous micron size particles broke into nanoscale fragments while sliding and the broken particle fragments accumulated within the worn surface of the polymer composite. Reinforcement of the sliding surface of the composite was achieved through accumulation of alumina particle fragments, chelated to tribochemically generated carboxylate metal salts. Only the porous micron-sized particles produced ultralow wear PTFE−α-Al_2O_3 composites, whereas dense and less friable fillers only achieved moderate wear rates.

It is a growing hypothesis that the formation of tribofilms on the wear surface is critical to the wear performance in PTFE−α-Al_2O_3 systems. Nanoindentation of the tribofilms on the wear surface of the polymer, or "running films", in ultralow wear PTFE−α-Al_2O_3 composites have been reported to have significantly higher modulus and hardness than the native PTFE or PTFE−α-Al_2O_3 surface.[22] A recent study by Van Meter et al. revealed that when the typically ultralow wear PTFE−α-Al_2O_3 composite is slid against itself, the ability to form this running film is impeded; this is accompanied by an increased wear rate as well as creep or other plastic deformation of the wear surface of the polymer.[27]

Past studies on PTFE−α-Al_2O_3 systems highlight the importance of tribofilms and suggest that micron-sized, dense, nonfriable fillers prevent tribofilm formation by abrading the countersurface.[18,23] A key characteristic of ultralow wear PTFE−α-Al_2O_3 composites is the formation of protective films on the worn surface of the composite and counterbody, resulting in reinforcement of the sliding interface due to particle accumulation during sliding.[21,22,28−30] However, how the specific mechanical properties of the alumina filler contribute to ultralow wear PTFE−Al_2O_3 systems is yet to be investigated. In this work, the apparent fracture toughness of different sets of dense and porous micron-sized alumina particles and an additional metal-oxide particle composite were evaluated directly using an in situ nanoindentation technique. The apparent fracture toughness of the metal-oxide particles was correlated with the wear properties of the PTFE−metal-oxide composite materials and tribochemical formation of tribofilms on the stainless steel counterbody and worn polymer surface. A mechanistic framework based on

https://doi.org/10.1021/acsami.2c13644
ACS Appl. Mater. Interfaces 2022, 14, 54293−54303

particle size and apparent fracture toughness was created to develop a metric to predict whether a particle will promote tribofilm formation or be abrasive to the counterbody.

2. RESULTS

In situ SEM nanoindentation was used to crush the metal-oxide filler particles and measure particle radius using the method outlined in Figures 1 and 2 and calculate apparent fracture toughness using eq 8 (see Materials and Methods section). Differences in the fracture force as a function of particle radius for each filler type are observed in Figure 3a and

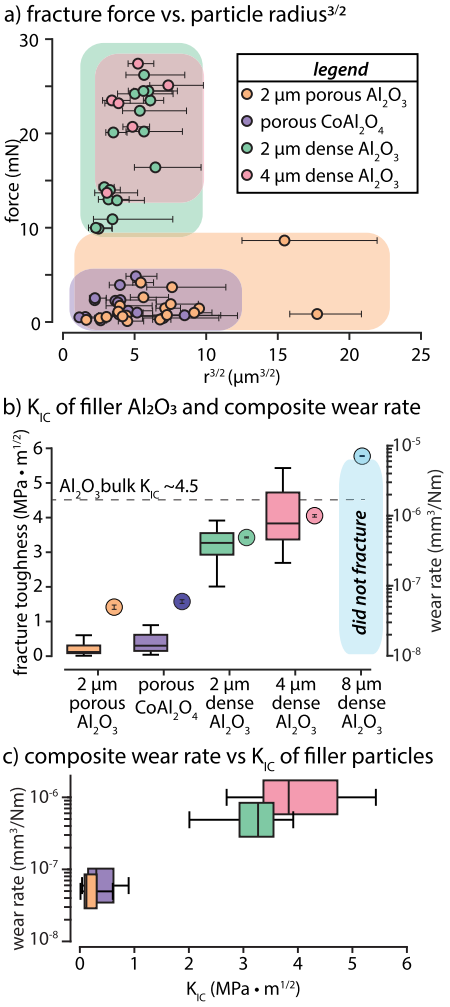

Figure 3. (a) Load measured at fracture vs estimated particle radius to the 3/2 power. (b) Estimated apparent fracture toughness of filler particles (boxes) and steady-state wear rate of PTFE-particle composites (circles). (c) Steady-state wear rate of PTFE-particle composites as a function of estimated apparent fracture toughness of filler particles.

show two groupings based on particle structure. The $CoAl_2O_4$ and porous 2 μm Al_2O_3 fractured at lower loads for all particle sizes compared to the dense 2 and 4 μm Al_2O_3 particles (Figure 3a). Figure 2 shows fracture of a representative porous alumina particle. It should be noted that the sample sizes are different for the filler materials, with all the $CoAl_2O_4$, porous 2 μm Al_2O_3, and dense 2 μm Al_2O_3 particles fracturing during indentation testing, while 47% of the dense 4 μm Al_2O_3 and 10% of the 8 μm Al_2O_3 fractured (Table 1). The $CoAl_2O_4$ and porous 2 μm Al_2O_3 particles have an apparent fracture toughness of 0.4 ± 0.30 MPa·$m^{1/2}$ (n = 16) and 0.21 ± 0.17 MPa·$m^{1/2}$ (n = 19), respectively. The dense 2 μm and dense 4 μm Al_2O_3 particles have a higher apparent fracture toughness (K_{IC} = 3.5 ± 0.6 MPa·$m^{1/2}$, n = 19 and K_{IC} = 4.4 ± 1.0 MPa·$m^{1/2}$, n = 17, respectively) with values close to that of bulk alumina Al_2O_3 (K_{IC} ~ 4.2−5.9 MPa·$m^{1/2}$[31]). Because of their larger size and apparent fracture toughness, only 2 out of 22 of the large, dense 8 μm Al_2O_3 particles fractured at the prescribed loads. As they are likely fully dense based on BET and static light scattering (SLS) measurements, it is assumed that they are near the fracture toughness of bulk alumina; as such, we would predict them to fail at loads greater than 100 mN, above the maximum achievable load on the indenter. A summary of the nanoindentation results is shown in Table 1.

The steady-state wear rate for each PTFE−metal-oxide composite clearly trends with the measured apparent fracture toughness of their respective filler particles (Figure 3b,c). The wear behavior for the PTFE-porous 2 μm Al_2O_3 composite, which has the lowest apparent particle fracture toughness, achieved an ultralow steady-state wear rate of 6.6 × 10^{-8} mm^3/Nm, approximately 10,000 times lower than unfilled PTFE. In contrast, the wear rate for the PTFE-dense 2 μm Al_2O_3 is approximately an order of magnitude higher than the porous particles with the friability functionality. PTFE filled with larger (4−7 μm) dense Al_2O_3 particles with apparent fracture toughness values similar to the fracture toughness of bulk Al_2O_3 have 10−100× higher wear rates than smaller porous filler particles and achieve steady-state wear rates of 9.7 × 10^{-7} mm^3/Nm (dense 4 μm Al_2O_3) and 7.1 × 10^{-6} mm^3/Nm (dense 8 μm Al_2O_3). Interestingly, to test the role of the friability functionality versus particle composition, a composite of PTFE and a friable $CoAl_2O_4$ composite were tested and show a similar ultralow wear rate (6.3 × 10^{-8} mm^3/Nm) to the PTFE-porous 2 μm Al_2O_3 composite.

The impact of apparent particle fracture toughness on the formation of protective transfer films is shown in Figures 4 and 5 through images and profilometry scans of the steel counterfaces. The transfer films formed by the PTFE−Al_2O_3 composite filled with porous, friable 2 μm Al_2O_3 and $CoAl_2O_4$ particles appear brown and uniform in coverage with no abrasion of the steel counterface, indicative of well-formed ultralow wear composite systems. Transfer films of composites filled with dense Al_2O_3 filler particles become patchy with the largest 8 μm Al_2O_3 filler particles preventing transfer film formation (Figures 4 and 5). Abrasive scratches start to form with the 2 μm dense Al_2O_3 particles and the countersurface is worn, with increasing particle size causing severe abrasion of the counterface forming deep grooves (~100−120 μm for the 8 μm particle) and generating large amounts of wear debris. The results from the images and profilometry scans of the steel counterbodies show that transfer film formation of a PTFE−metal-oxide composite is dependent on the apparent fracture toughness and size of the filler particles, which impacts the wear performance of the tribological system.

Attenuated total reflectance infrared spectroscopy (ATR-IR) was performed on the unworn composite surface (Figure 6a) and worn composite surface (Figure 6b) after all tests were completed to understand the role of the apparent fracture toughness of the particle filler on the formation of tribochemical species at the sliding interface. The spectra of all five unworn composites revealed two peaks at 1159 and 1216 cm^{-1} corresponding to CF_2 bonds. The shoulder of the

https://doi.org/10.1021/acsami.2c13644
ACS Appl. Mater. Interfaces 2022, 14, 54293−54303

Table 1. Results from Tribology and Nanoindentation Experiments[a]

particle	BET		SLS			tribological results			indentation results		
shorthand name	A_S, m^2/g	r, μm	r_{25}, μm	r_{50}, μm	r_{75}, μm	μ_{ss}	wear rate (mm^3/Nm)	worn volume (mm^3)	N particles	% fractured	K_{IC} ($MPa{\cdot}m^{1/2}$)
2 μm porous Al_2O_3	41.4	0.02	1.0	2.1	3.6	0.21	$6.6 \times 10^{-8} \pm 0.3 \times 10^{-8}$	0.7	19	100	0.21 ± 0.17
2 μm dense Al_2O_3	2.3	0.33	1.3	2.2	3.2	0.22	$4.2 \times 10^{-8} \pm 0.1 \times 10^{-7}$	5.6	19	100	3.5 ± 0.63
4 μm dense Al_2O_3	0.34	2.21	3.1	4.1	4.8	0.27	$9.7 \times 10^{-8} \pm 0.3 \times 10^{-7}$	31.0	17	47	4.2 ± 1.0
8 μm dense Al_2O_3	0.12	6.35	6.0	7.7	9.3	0.39	$7.1 \times 10^{-8} \pm 0.1 \times 10^{-6}$	36.1	22	9	N/A
1 μm porous $CoAl_2O_4$	5.8	0.13	0.5	0.8	1.3	0.24	$6.3 \times 10^{-8} \pm 0.3 \times 10^{-8}$	1.2	16	100	0.41 ± 0.31

[a]Friction coefficient (μ) reported is the average of the entire experiment. Wear rate ($K_{\text{Monte Carlo}}$) reported was determined using the technique developed by Schmitz et al.[32] The number of particles indented (n), the percentage of particles fractured (% fractured), and estimated apparent fracture toughness (K_{IC}) of the different particles have also been reported.

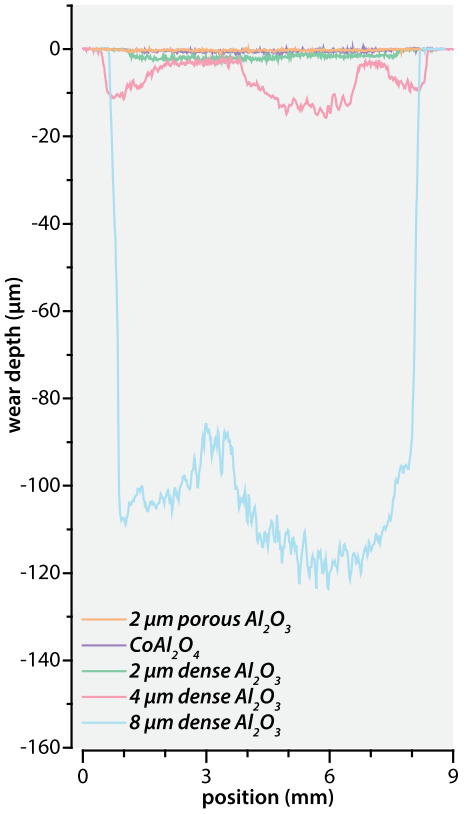

Figure 4. Worn surface profile of the 304L SS counterbody and polymeric transfer film measured by scanning white light interferometry scans across the worn surfaces of the 304L SS counterbody. The right-hand side of the figure shows images of the 304L SS counterbody after 25 km of sliding. Dotted lines on the pictures of the counterbodies in Figure 5 indicate where each scan was taken.

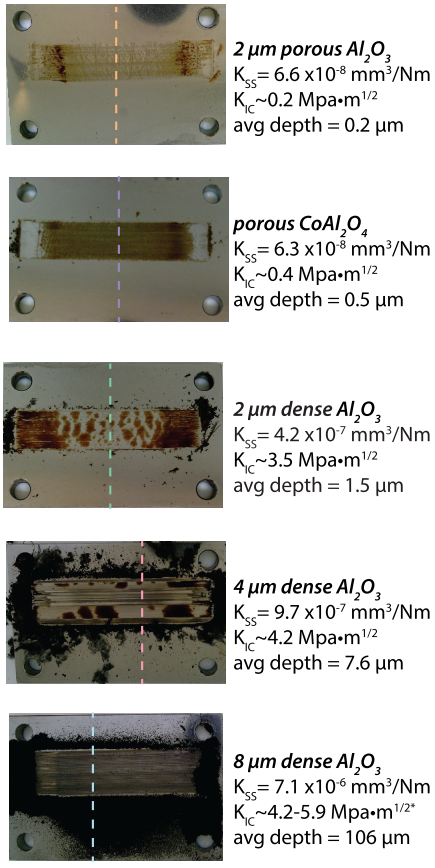

Figure 5. Images of the 304L SS counterbody and polymeric transfer film after 25 km of sliding. Dotted lines on the pictures of the counterbodies indicate where each scan in Figure 4 was taken. *Note: K_{IC} values were unable to be determined experimentally for this particle size. K_{IC} was assumed to be equivalent to bulk alumina.[31]

infrared spectra under 900 cm^{-1} corresponds to metallic oxides (alumina or cobalt aluminate). The infrared spectra after sliding for all five composites were similar in character (Figure 6b). All five composites had strong absorbance peaks at 1434 and 1665 cm^{-1} corresponding to the formation of carboxylate salts. There is an increase in the signal both within the metallic oxide region (500−900 cm^{-1}) and waters of hydration (broad peak between 2900 and 3600 cm^{-1}). The diminished signals for the PTFE-dense 8 μm alumina spectra are due to poor reflectance of the worn surface, which is covered with metallic wear debris (Figure 7).

3. DISCUSSION

3.1. Tribological Mechanistic Framework for Ultralow Wear PTFE−Alumina Composites. All worn composite surfaces exhibited the tribochemical formation carboxylate salt groups based on the ATR-IR results (Figure 6b). Throughout the literature of ultralow wear PTFE−alumina composites, this chemical species and IR spectra have been characteristic and indicative of ultralow wear PTFE systems.[20,21,33−36] However, there is a 10−100× difference in wear rate from a friable alumina particle (porous 2 μm Al_2O_3; $K_{IC} \sim 0.21$ $MPa{\cdot}m^{1/2}$) to a fully dense alumina particle (near bulk fracture toughness)

https://doi.org/10.1021/acsami.2c13644
ACS Appl. Mater. Interfaces 2022, 14, 54293−54303

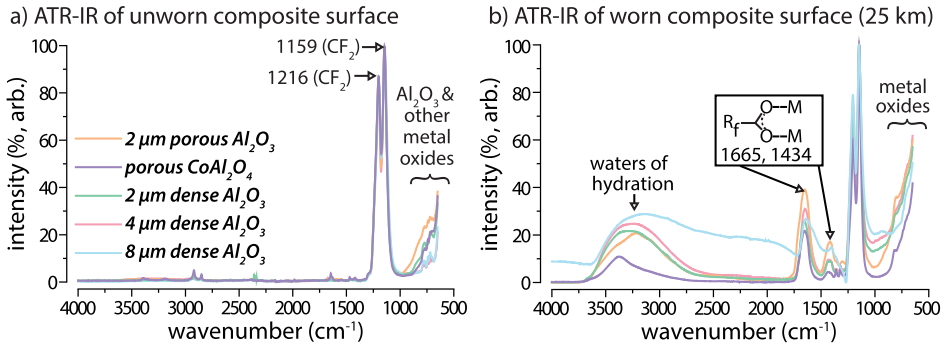

Figure 6. (a) ATR-IR spectra of the unworn PTFE–metal-oxide composite surfaces. (b) ATR-IR spectra of the worn PTFE–metal-oxide composite surfaces after 500k cycles (25 km).

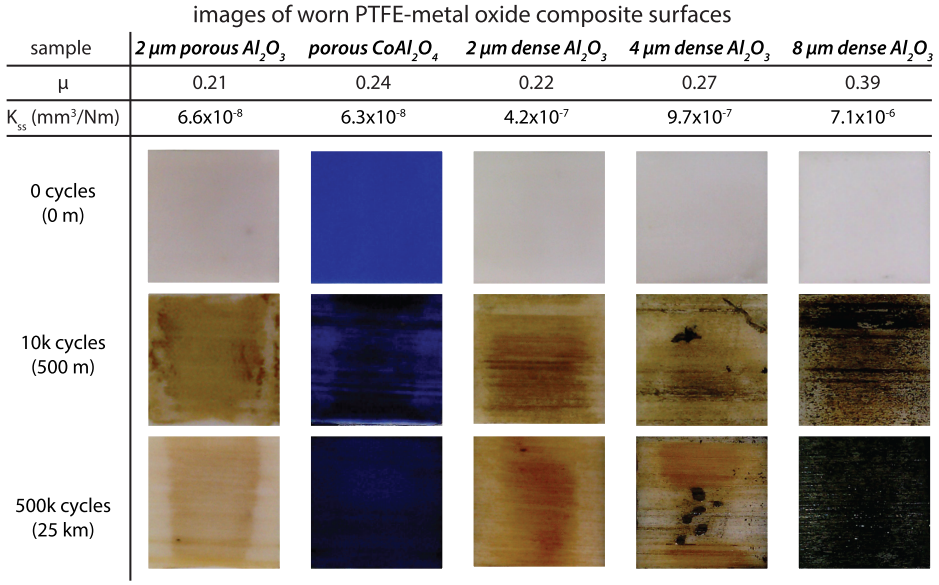

Figure 7. Images of the PTFE–metal-oxide composites before sliding, at 10k cycles (500 m), and after all tests were completed (500k cycles; 25 km).

particles depending on the filler particle size. This is direct evidence that while the tribochemical reaction with PTFE and water vapor is imperative for this system to be ultralow wear,[21,35−39] it is not a sole indicator of the ultralow wear state. Thus, additional functionalities of the filler must be considered. It is observed that the wear rate of the composites tested increases monotonically with the apparent fracture toughness of the filler particle used, indicating that the wear reduction phenomenon depends on the particles' ability to maintain a tribofilm and prevent severe abrasion of the counterbody by breaking up during sliding. In the present work, we suggest that additional functionality is that where the filler particle is friable to break during sliding and incorporate into tribofilms in situ during sliding.

IR spectroscopy of the composite wear surface also demonstrates that filler particles accumulate at the sliding interface during sliding, regardless of apparent fracture toughness of the filler particle. This increases the frequency of contact between filler particles and the countersurface. Krick et al. showed that the porous 2 μm Al_2O_3 particles (demonstrated in the present work to have lower apparent fracture toughness) accumulate as nanoscale fragments at the wear surface of the polymer.[23] In another paper, Krick et al. reported that the hardness of these surface layers in ultralow wear PTFE–alumina composites reinforced by sliding is approximately 3 times higher than the unworn surface.[22] We hypothesize that these nanoscale filler fragments are bound to the surface through the carboxylate end groups formed tribochemically during sliding, further strengthening the surface.

In the case where the particles cannot fracture, dense, tough particles accumulate at the sliding interface and abrade the transfer film. These differences in abrasion are observed in profilometry scans of the steel counterface with the PTFE-dense 8 μm Al_2O_3 composite showing deep groves (~100 μm) and severe abrasion of the steel, while the steel countersurface of the PTFE-porous 2 μm Al_2O_3 composites did not wear. The dense 8 μm Al_2O_3 particles (which mostly remained unfractured in our nanoindentation experiments) accumulate at the sliding interface abrading any generated tribofilm on the countersurface (Figures 4 and 5) resulting in a ~10× increase in wear rate over composites with porous friable filler particles. If the transfer film is not replaced by the worn material adhering to the steel countersample, the particles begin to abrade the steel as well; with continued sliding without transfer film formation, the counterbody becomes scratched with aligned grooves in the sliding direction (Figures 4 and 5), which has been shown by Harris et al. to result in increased

https://doi.org/10.1021/acsami.2c13644
ACS Appl. Mater. Interfaces 2022, 14, 54293−54303

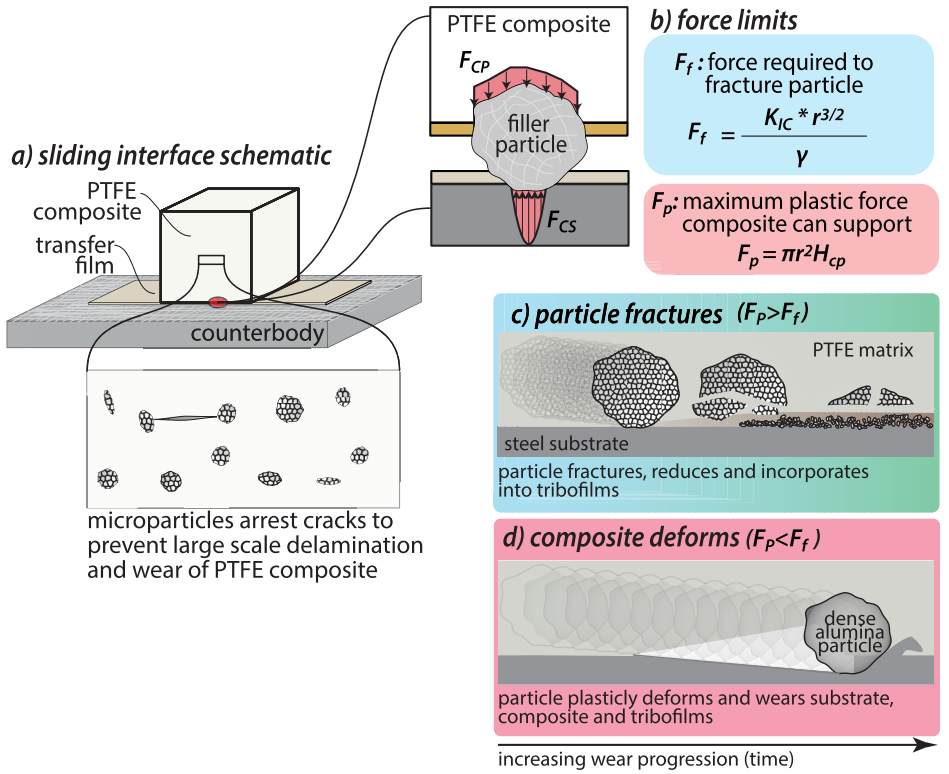

Figure 8. Filler particle interaction with composite and counterbody. (a) PTFE composite sliding against metal counterbody with inset showing the interface of the composite, counterbody, and particle. Here, the particle has a compressive reaction force with the composite (F_{CP} by integrating the contact pressure) and a compressive reaction force with the countersample (F_{CP}), which are equal when in equilibrium. (b) Definition of the force required to fracture a particle (F_f) and the maximum plastic force the composite can support (F_p). (c) Particle fracture likely occurs when $F_p > F_f$. This helps reduce the abrasiveness of the particles, and the smaller particles incorporate into the tribofilms. (d) When $F_f > F_p$, particle fracture is unlikely. This likely causes deformation of the PTFE composite and abrasion of the countersample.

wear of the composite due to increased difficulty of tribofilm retention.[19] In the experiments performed in the current study, the PTFE with dense 8 μm Al_2O_3 composites caused grooves along the sliding direction, resulting in an aligned roughness topography on the counterbody surface over time, leading to a wear rate increasing from 3.7×10^{-7} mm^3/Nm after 250 m to 7.1×10^{-6} mm^3/Nm, similar to wear rates of PTFE−alumina when slid against parallel surface grooves reported by Harris et al. (9.6×10^{-6} mm^3/Nm). By using friable, less abrasive filler particles, the rate of transfer film deposition matches or exceeds the rate at which the surface is being abraded.

When choosing a filler material, fracture toughness of the particles should be considered as they allow for less surface abrasion and the promotion of protective transfer films. The $CoAl_2O_4$ particles in the present study were selected to test this hypothesis as previous electron micrographs showed that they were porous, thus assumed to be friable. As expected, they were friable with a low-apparent fracture toughness (0.41 MPa·m$^{1/2}$) and astonishingly resulted in ultralow wear performance, significantly lower than the dense Al_2O_3 particles that had apparent fracture toughness values close to bulk Al_2O_3 (~4.5 MPa·m$^{1/2}$).

Mechanistically, the friable particles perform several functions. They must first prevent the delamination wear mode of PTFE, which can be achieved by compositing PTFE with nearly any microscale filler[4,6,7,9,10] (Figure 8a). Second, there may be some element of promotion of tribochemistry.[30,40−42] Finally, in the present work, we show that they break into smaller fragments (Figure 8c), helping form and reinforce thin tribofilms. Thus, the separating functionality of the microscale filler particles that produce ultralow wear PTFE composites is their ability to break into fragments during sliding and form protective tribofilms that result in ultralow wear rates, whereas large, dense particles abrade the surface removing any transfer film and scratching the steel counterface (Figure 8d).

3.2. Metric for Brittle Fillers Functionality in Ultralow Wear PTFE-Oxide Composites. The goal of this work is to create a framework that allows for the selection and design of filler particles for PTFE composites that is not based on purely empirical tribological testing of different composites composed of different fillers. Using the relationships, we observed between apparent particle fracture toughness, wear rate, and tribofilm formation we create a model to predict if a filler particle will result in ultralow wear (Figures 8 and 9). Filler particles were trapped at the interface of the PTFE composite and steel counterbody during sliding, with each particle supporting some portion of the normal load and having a force exerted on the particle (F) which may cause two events to occur (Figure 8a). The first event is when the force on the particle is greater than the force required to fracture the particle (F_f) ($F > F_f$), causing the particle to break into smaller fragments (Figure 8c). F_f may be determined by rearranging eq 8 (see Materials and Methods section) as shown in eq 1

$$F_f = \frac{K_{IC} \times r^{3/2}}{\gamma} \quad (1)$$

https://doi.org/10.1021/acsami.2c13644
ACS Appl. Mater. Interfaces 2022, 14, 54293−54303

Alternatively, the force on the particle may exceed the plastic capacity of the composite (F_p) and plow into the composite surface (Figure 8d). F_p is defined using the hardness of the composite (H_{cp}) and the projected area of the filler particle (A_{proj}) (eq 2).

$$F_p = H_{cp} \times A_{proj} = H_{cp} \times \pi r^2 \tag{2}$$

The ratio of F_p/F_f can be used to estimate the likelihood that a metal-oxide particle breaks or if the composite is damaged (eq 3).

$$\frac{F_p}{F_f} = \frac{H_{cp} \times \pi r^2}{\frac{K_{IC} \times r^{3/2}}{\gamma}} = \gamma \times \pi \times \left(\frac{H_{cp}}{K_{IC}}\right)(r)^{0.5} \tag{3}$$

When the ratio of F_p/F_f is greater than 1, the maximum force the composite can apply to the particle is greater than the force required to fracture the particle and the particle will break up during sliding. Past work on the same PTFE−α-Al_2O_3 composite used here (2 μm porous Al_2O_3) showed via TEM of the worn polymer composite surface that the porous particles broke down to on the order of 100 nm during sliding.[23] When $F_p/F_f < 1$, the maximum force the composite can apply to the particle is less than the force required to fracture the particle, resulting in deformation of the polymer and interfacial particles remaining intact. Fracture of the filler particle over plastic deformation of the composite is the ideal mechanism for ultralow wear as smaller particles are less abrasive to the counterbody and the composite. Based on eq 3, particles with lower apparent fracture toughness for a given diameter and composite hardness result in less abrasion of the counterbody and wear of the composite.

Krick et al. found the hardness of the wear surface of PTFE Al_2O_3 to be 145 MPa.[22] Based on the similar conditions of that study and this set of experiments, the hardness of the worn PTFE−α-Al_2O_3 and PTFE−$CoAl_2O_4$ composite will be assumed to be ∼145 MPa as well. With this assumption, the required apparent fracture toughness (K_{IC}) of the particle for a given particle diameter is determined. Over a range of expected particle radii (0.1−100 μm), the K_{IC} value required for F_p/F_f = 1 was determined and is plotted in Figure 9. The left-hand side of the line that meets the criteria F_p/F_f = 1 indicates that particle fracture is more probable ($F_p/F_f > 1$), while the right-hand side of this line suggests that plastic deformation of the polymer composite dominates over particle fracture ($F_p/F_f < 1$). We use the hardness of the run-in, ultralow wear PTFE wear surface for the failure criteria as it is harder than that of the unworn composite, so we expect that the system is generally getting harder as fillers accumulate at the wear surface. We recognize that if we used the hardness of steel, it would shift the entire line in Figure 9 down. However, it has been repeatably observed that stable tribofilms must be formed in order for the system to remain ultralow wearing,[33] thus the most meaningful hardness metric is that of the run-in, ultralow wear PTFE composite.

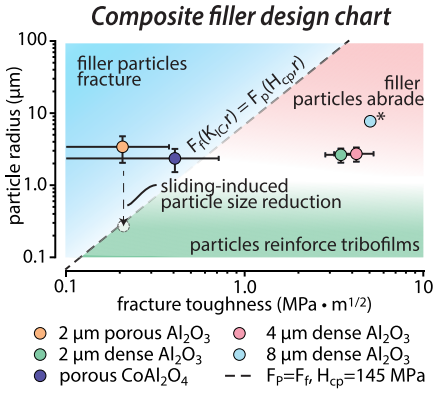

Figure 9. PTFE composite filler design chart. Dotted line represents when $F_f = F_p$. Particle fracture likely occurs when $F_p > F_f$. This helps reduce the abrasiveness of the particles, and the smaller particles incorporate into the tribofilms. When $F_f > F_p$, particle fracture is unlikely. This likely causes deformation of the PTFE composite and abrasion of the countersample. *Apparent fracture toughness of the 8 μm dense Al_2O_3 particle assumed to be equal to the bulk fracture toughness of alumina (4.5 MPa·m$^{1/2}$) as particles did not fracture under the prescribed loads.

Particles to the left of the F_p/F_f = 1 line ($CoAl_2O_4$ and 2 μm porous Al_2O_3) are going to fracture into smaller particles. This reduction in particle size prevents abrasion of the transfer film on the counterbody (Figures 4 and 5). The 2 μm dense Al_2O_3, 4 μm dense Al_2O_3, and 8 μm dense Al_2O_3 particles are to the right of the equal force line and are unlikely to fracture. The inability of these particles to fracture and remain intact causes abrasion during sliding, which is shown to varying degrees in Figures 4 and 5. When using Figure 9 as a guide to select other possible materials, low-apparent fracture toughness particles (K_{IC} ∼ 0.1−1.0 MPa·m$^{1/2}$) that are near 10 μm in size would fracture as well. Materials such as glasses and silicon have fracture toughness values in that range and may be used to evaluate this theory further.[31] The authors would like to caution their audience that the wear of PTFE composite systems has additional factors, such as tribochemical reactions[37,42,43] and the formation of transfer films[25,29] that this theory does not consider. New filler materials may be likely to fracture but may not promote tribofilm formation on the counterbody like the porous Al_2O_3 or $CoAl_2O_4$ particles. However, if the selected particles can form chemical bonds to the broken PTFE chains created during sliding, this theory would aid them in choosing between which particles would be more likely to promote lower wear.

There is a limit in particle size when apparent fracture toughness becomes less important as particles reach a size that is small enough to not abrade away the stainless steel counterbody but are large enough to prevent large-scale delamination of the PTFE matrix. This region is ideal as the particles can act as mechanical reinforcement and sites for tribochemical bonding without being large enough to damage the counterbody. There is also a lower limit in particle size where particles are too small (near 10−40 nm in radius) and will not mechanically reinforce the PTFE matrix. This is supported by studies on PTFE filled with nano-alumina by Burris and Sawyer,[16] which found that only 80 nm diameter α Al_2O_3 was able to reduce wear by 3 orders of magnitude. Smaller alumina particles (between 38 and 50 nm in diameter) were only modestly able to improve the wear of the composite. Additional studies on PTFE−Si_3N_4 and PTFE−γ-Al_2O_3 composites by Bhargava and Blanchet found that micron-sized Si_3N_4 and γ-Al_2O_3 filler particles improved the wear of PTFE systems by 2 orders of magnitude, while nanofillers of the same materials did not improve wear significantly or at all compared to unfilled PTFE.[44]

https://doi.org/10.1021/acsami.2c13644
ACS Appl. Mater. Interfaces 2022, 14, 54293−54303

4. CONCLUSIONS

Friable nanostructured alumina microparticles have added functionality over fully dense alumina microparticles when added to PTFE for tribological applications, resulting in 10,000 times improvements in the wear of PTFE. These filler particles are able to mechanically reinforce PTFE through traditional mechanisms as well as the additional ability of being able to break into nanoscale fragments within the tribofilms formed on the wear surface of the composite as well as the countersample (transfer film). A quantitative model that compares the likelihood of the filler to fracture versus it plastically deforming the wear surface during sliding was presented to predict fillers that can achieve ultralow wear, using the apparent fracture toughness of filler particles, as measured by nanoindentation. The best performing system was porous alumina particles ~2 μm average size, with low-apparent fracture toughness (K_{IC} ~ 0.21 MPa·m$^{1/2}$); based on this, friable $CoAl_2O_4$ particles (K_{IC} ~ 0.41 MPa·m$^{1/2}$) of ~1 μm average size were successfully predicted to have ultralow wear. Composites made with higher apparent fracture toughness particles of varying size had higher wear rates with increasing particle size due to the increasing likelihood of particles (typically sold for polishing applications) to abrade the countersamples protective transfer films; the fracture model predicted that these larger particles would not break during sliding and produce higher wear rates, as they did. Though all systems observed similar tribochemical groups, PTFE composites with lower apparent fracture toughness filler particles were able to maintain transfer films and not abrade the countersurface. This particle fracture model may be used to help identify future filler materials for PTFE that would not abrade the countersurface while promoting mechanical and chemical reinforcement of the worn polymer surface.

5. MATERIALS AND METHODS

5.1. Metal-Oxide Particle Characterization. The metal-oxide particles were selected based on commercial availability and particle morphology (Table 2). Multiple vendors were used to get a range of size and morphology, including Nanostructured & Amorphous Materials, Inc. (Katy, TX), Pace Technologies (Tucson AZ), and Ferro Corporation (King of Prussia, PA). Nitrogen gas adsorption tests were used to determine the specific surface area of each of the particle types tested using the BET method.[45] An estimated particle radius for assumed fully dense, monodisperse spherical particles may be calculated using the following assumptions. First, the specific surface area, A_S, of a sphere may be estimated using eq 4

$$A_S = \frac{4\pi r^2}{m} \tag{4}$$

where m is the mass of the sphere and r is the particle radius. In a similar fashion, the specific volume, V_S, of a sphere (eq 5) is defined as

$$V_S = \frac{\frac{4}{3}\pi r^3}{m} \tag{5}$$

The "BET particle radius" can be calculated by dividing the specific volume (eq 5) by the specific surface area (eq 4) and solving for r, resulting in eq 6.

$$r = 3\frac{V_S}{A_S} \tag{6}$$

Typically, the specific volume is assumed based on the density of the bulk metal-oxide materials, while the specific surface area is measured by the BET gas adsorption measurements. This means that BET often under predicts particle radius, especially in porous and nonspherical particles.

Table 2. Properties of Particles Used in This Study Including a Shorthand Particle Name, Vendor Name, Stock Number, Vendor-Reported Particle Size

particle	vendor-supplied information		
shorthand name	vendor	stock #	Vendor-reported size (μm)
2 μm porous Al_2O_3	Nanostructured & Amorphous Materials, Inc.	1015WW	0.014−0.022
2 μm dense Al_2O_3	Pace Technologies	ALR-0150-05	2.5
4 μm dense Al_2O_3	Pace Technologies	ALR-1200-05	6
8 μm dense Al_2O_3	Pace Technologies	ALR-2000-05	10
1 μm porous $CoAl_2O_4$	Ferro Corporation	PB28, V-3285	0.75−1.0

Particle size was measured directly using SLS measurements. The results of the particle sizes for the five sets of polymer composites tested are shown in Table 1. The mean particle size for SLS compared to the estimated particle size by BET shows the relative porosity of the particles. For example, porous 2 μm Al_2O_3 had an estimated particle radius of 18 nm by BET, while SLS estimated its particle radius to be 2.08 μm. This 100 times difference is likely due to porosity within the particle, which was confirmed by SEM. The other particles did not show nearly as large of differences between the BET- and SLS-estimated radii and therefore were not much porous.

5.2. Sample Preparation. Chemours (formerly DuPont) PTFE 7C powder (~30 μm particles) was mixed with each filler material by hand at a ratio of 5 wt% filler/95 wt % PTFE. Isopropanol was added to the PTFE and filler particle mixture at a 2:1 ratio of alcohol to powder. This mixture was further mixed using Branson Digital Sonifier SFX 550 (Emerson Electric Co., St. Louis, MO, USA) with a 1/8″ microtip attachment for 5 min. After mixing, the mixtures were allowed to dry for 1 week. The composite mixtures were then cold-pressed into 12.7 mm diameter cylinders using a hydraulic press with compressive stresses on the cylinders ranging from 50 to 100 MPa. These cylinders were sintered in lab air by heating at 120 °C/h, held at 380 °C for 3 h, and cooled at 120 °C/h. After sintering, the cylinders were machined into 12.7 mm × 6.3 mm × 6.3 mm and wet ground using 800 grit SiC paper. All samples were then cleaned in an ultrasonicating methanol bath for 30 min. The countersurface material for all tests was lapped 304L stainless steel (R_a ~ 150 nm). Each countersurface was washed in soap and water (Alconox Powder Precision Cleaner) and then wiped with methanol at least 30 min before testing began.

5.3. Tribological Measurements. A linear reciprocating tribometer as described previously by Schmitz et al.[32] was used to evaluate the friction coefficient and wear rate of the different PTFE−metal-oxide composites. The steady-state wear rate of the PTFE metal-oxide composites was calculated using the methods outlined by Schmitz et al. as well[32]

$$K\left[\frac{\text{mm}^3}{\text{N m}}\right] = \frac{V_{lost}}{F_n \cdot d} = \frac{\Delta m L_1 L_2 L_3}{2F_n m_i SN} \tag{7}$$

where $V_{lost} = \Delta m/\rho_s$, $d = 2SN$ is the total sliding distance, Δm is the mass change in the sample due to wear, $\rho_s = m_i/V_S$ is the sample density, m_i is the initial mass of the sample, $V_S = L_1L_2L_3$ is the initial volume of the sample, S is the stroke in each cycle, and N is the number of bidirectional cycles. Friction coefficients for each composite were determined using the methods outlined by Burris and Sawyer.[46] A 250 N normal load was applied (~6.3 MPa contact pressure) to each sample, and each sample was slid at a rate of 50 mm/s with a stroke length of 25 mm. Mass measurements were taken before testing and after the following amount of cycles were completed: 1k, 2k, 3k, 4k, 5k, 10k, 20k, 30k, 40k, 50k, 100k, 200k,

https://doi.org/10.1021/acsami.2c13644
ACS Appl. Mater. Interfaces 2022, 14, 54293−54303

300k, and 500k corresponding to a total distance slid of 25 km. A balance with 10 μg precision was used for all mass measurements (Mettler-Toledo XSR205, Greifensee, Switzerland).

5.4. Transfer Film Measurements. To measure the height of the surface films across the PTFE composites, a scanning white light interferometer (Bruker GT-K, Billerica MA, USA) was used. Profiles of 9 mm length were stitched together across the transfer films, making sure to include unworn metal counterface on each side of the measurement. The location of the scans was near the middle section of the wear track.

5.5. Attenuated Total Reflectance Infrared Spectroscopy. The chemical composition of the unworn and worn (after 25 km of testing) PTFE−metal-oxide composite surfaces was evaluated using ATR-IR. A Spectrum 1000 infrared spectrometer (PerkinElmer, Waltham, MA) was used for all spectra. Each spectrum presented is an average of 16 scans that were taken from 650 to 4000 cm^{-1} with a resolution of 4 cm^{-1}. The surface of interest was pressed against a diamond crystal. The crystal was cleaned between each measurement, and a new background scan was acquired.

5.6. Apparent K_{IC} Estimation Using Nanoindentation. The mechanical properties of each of the metal-oxide particles composited with PTFE were evaluated using an in situ nanoindenter (PI-85 Picoindentor, Hysitron, Eden Prairie, MN USA) mounted onto a JEOL JSM-IT300HR scanning electron microscope (Tokyo, Japan) at the Sandia National Laboratories Center for Integrated Nanotechnologies (CINT) user facility. The nanoindenter was equipped with a diamond cube-corner indenter. Each metal-oxide particle type was deposited on a polished sapphire wafer (12.7 mm diameter, 0.5 mm thick) using a pipette filled with a dilute solution of isopropanol and the metal-oxide particle. The dilute mixture was sonicated for 30 min before deposition to avoid agglomeration of particles. Each particle was indented using the following indentation profile: increasing load to 0.3 mN for 10 s, decreasing load to 0 mN for 10 s, increasing load to 3 mN for 10 s, decreasing load to 0 mN for 10 s, increasing load to 30 mN for 10 s, and decreasing load to 0 mN. 30 mN is the maximum achievable load on the nanoindenter. Sebastiani et al. developed a model that calculates the fracture toughness of ceramic micropillars with a Berkovich tip[47] (eq 8). Work by Ghidelli et al. extended the model to indentation performed with a cube-corner tip.[48] The model presented estimates the fracture toughness based on the coefficient γ, fracture load at failure (F_f), and the radius of the cylinder (r) (eq 8).[48]

$$K_{IC} = \frac{\gamma \cdot F_f}{r^{3/2}} \tag{8}$$

The coefficient γ is a function of the tip geometry and the ratio of the elastic modulus (E) and hardness (H) of the particle. Ghidelli et al. calculated γ for a range of E/H ratios for cube-corner indenter tips. The elastic modulus and hardness of alumina were taken to be 392 GPa and 19.25 GPa, respectively,[49] which correspond to a γ value of 0.79. Similarly, the modulus and hardness of cobalt aluminate were 256.8 GPa and 15.5 GPA, respectively, which result in a γ value of 0.75.[50] A graphic overview of the nanoindentation experiments is shown in Figures 1 and 2.

In this paper, we assume that these particles, which are of similar size and shape to the pillars used in Ghidelli et al., behave similarly to micropillars. This is only a rough first-order approximation since there are obvious differences in the shape of the particle and its attachment to the substrate, compared to micropillars. An approximate radius was calculated for each particle based on SEM micrographs (Figure 2b). Using the MATLAB image processing toolbox, particles were identified, and an ellipse was fit to each particle with the major axis and minor axis lengths calculated. The average particle diameter, assumed to be a circle, was calculated as an equivalent diameter from the area of the ellipse. The error in particle diameter shown in Figure 3a, and used for calculations, is based on particles that have a diameter equivalent to either the major or minor axis of the fit ellipse.

AUTHOR INFORMATION

Corresponding Author

Brandon A. Krick − *Department of Mechanical Engineering, Florida A&M University-Florida State University College of Engineering, Tallahassee, Florida 32310, United States;* orcid.org/0000-0003-3191-5433; Email: bkrick@eng.famu.fsu.edu

Authors

Mark A. Sidebottom − *Department of Mechanical and Manufacturing Engineering, Miami University, Oxford, Ohio 45056, United States*

Tomas F. Babuska − *Sandia National Laboratories, Albuquerque, New Mexico 87185, United States; Department of Mechanical Engineering and Mechanics, Lehigh University, Bethlehem, Pennsylvania 18015, United States; Department of Mechanical Engineering, Florida A&M University-Florida State University College of Engineering, Tallahassee, Florida 32310, United States*

Sifat Ullah − *Department of Mechanical and Manufacturing Engineering, Miami University, Oxford, Ohio 45056, United States*

Nathan Heckman − *Sandia National Laboratories, Albuquerque, New Mexico 87185, United States*

Brad L. Boyce − *Sandia National Laboratories, Albuquerque, New Mexico 87185, United States*

Complete contact information is available at: https://pubs.acs.org/10.1021/acsami.2c13644

Notes

The authors declare no competing financial interest.

The data that support the findings are available in the manuscript and are maintained by the corresponding author. Data are available upon request.

ACKNOWLEDGMENTS

This material is based on the work supported by the National Science Foundation CMMI MEP #2027029 (Krick CAREER), the National Science Foundation CMMI MEP #1463141 (Krick GOALI), and the National Science Foundation Graduate Research Fellowship Program under grant #1842163 (Babuska). The in situ nanoindentation experiments were performed at the Center for Integrated Nanotechnologies, a Department of Energy Office of Basic Energy Sciences User Facility. Sandia National Laboratories is a multi-mission laboratory managed and operated by National Technology and Engineering Solutions of Sandia, LLC., a wholly owned subsidiary of Honeywell International, Inc., for the U.S. Department of Energy's National Nuclear Security Administration under contract DE-NA0003525. This paper describes objective technical results and analysis. Any subjective views or opinions that might be expressed in the paper do not necessarily represent the views of the U.S. Department of Energy or the United States Government. The authors would like to thank Greg Blackman and Heidi Burch (DuPont) and Chris Junk (CJIdeas) for years of collaborations, debates, and passionate discussions on this topic. The authors would like to thank Faysal Haque and Sarah Herbruck of Miami University for discussion on the fracture model. Additionally, the authors thank Claudia Kolanovic for her help with the tribology experiments and data analysis. The authors would also like to thank Khalid Hattar of the Center for Integration of

https://doi.org/10.1021/acsami.2c13644
ACS Appl. Mater. Interfaces 2022, 14, 54293−54303

Nanotechnology for his help with the nanoindentation experiments. This work was supported by the Miami University the Faculty Research Grant program.

REFERENCES

(1) Ebnesajjad, S.*Fluoroplastics: Volume 1 Non-Melt Processible Fluoropolymers*; Elsevier, 2015.
(2) Ünlü, B. S.; Atik, E.; Köksal, S. Tribological properties of polymer-based journal bearings. *Mater. Des.* **2009**, *30*, 2618.
(3) Tevrüz, T. Tribological behaviours of bronze-filled polytetrafluoroethylene dry journal bearings. *Wear* **1999**, *230*, 61.
(4) Blanchet, T. A.; Kennedy, F. E. Sliding wear mechanism of polytetrafluoroethylene (PTFE) and PTFE composites. *Wear* **1992**, *153*, 229−243.
(5) Biswas, S. K. K.; Vijayan, K. Friction and wear of PTFE - a review. *Wear* **1992**, *158*, 193−211.
(6) Uchiyama, Y.; Tanaka, K. Wear laws for polytetrafluoroethylene. *Wear* **1980**, *58*, 223−235.
(7) De-Li, G.; Bing, Z.; Qun-Ji, X.; Hong-Li, W. Effect of tribochemical reaction of polytetrafluoroethylene transferred film with substrates on its wear behavior. *Wear* **1990**, *137*, 267−273.
(8) Biswas, S. K.; Vijayan, K. Changes to near-surface region of PTFE during dry sliding against steel. *J. Mater. Sci.* **1988**, *23*, 1877.
(9) Tanaka, K.; Kawakami, S. Effect of various fillers on the friction and wear of polytetrafluoroethylene-based composites. *Wear* **1982**, *79*, 221.
(10) Burris, D. L.; Zhao, S.; Duncan, R.; Lowitz, J.; Perry, S. S.; Schadler, L. S.; Sawyer, W. G. A route to wear resistant PTFE via trace loadings of functionalized nanofillers. *Wear* **2009**, *267*, 653−660.
(11) Nak-Ho, S.; Suh, N. P. Effect of fiber orientation on friction and wear of fiber reinforced polymeric composites. *Wear* **1979**, *53*, 129−141.
(12) Lancaster, J. K. Polymer-based bearing materials—The role of fillers and fibre reinforcement in wear. *Wear* **1972**, *22*, 412.
(13) Bahadur, S.; Tabor, D. The wear of filled polytetrafluoroethylene. *Wear* **1984**, *98*, 1−13.
(14) Li, F.; Hu, K.-a.; Li, J.-l.; Zhao, B.-y. The friction and wear characteristics of nanometer ZnO filled polytetrafluoroethylene. *Wear* **2001**, *249*, 877−882.
(15) Chen, W. X.; Li, F.; Han, G.; Xia, J. B.; Wang, L. Y.; Tu, J. P.; Xu, Z. D. Tribological behavior of carbon-nanotube-filled PTFE composites. *Tribol. Lett.* **2003**, *15*, 275.
(16) Burris, D. L.; Sawyer, W. G. Improved wear resistance in alumina-PTFE nanocomposites with irregular shaped nanoparticles. *Wear* **2006**, *260*, 915−918.
(17) Sidebottom, M. A.; Pitenis, A. A.; Junk, C. P.; Kasprzak, D. J.; Blackman, G. S.; Burch, H. E.; Harris, K. L.; Sawyer, W. G.; Krick, B. A. Ultralow wear Perfluoroalkoxy (PFA) and alumina composites. *Wear* **2016**, *362*−*363*, 179.
(18) McElwain, S. E.; Blanchet, T. A.; Schadler, L. S.; Sawyer, W. G. Effect of particle size on the wear resistance of alumina-filled PTFE micro- and nanocomposites. *Tribol. Trans.* **2008**, *51*, 247.
(19) Harris, K. L.; Curry, J. F.; Pitenis, A. A.; Rowe, K. G.; Sidebottom, M. A.; Sawyer, W. G.; Krick, B. A. Wear Debris Mobility, Aligned Surface Roughness, and the Low Wear Behavior of Filled Polytetrafluoroethylene. *Tribol. Lett.* **2015**, *60*, 2.
(20) Pitenis, A. A.; Harris, K. L.; Junk, C. P.; Blackman, G. S.; Sawyer, W. G.; Krick, B. A. Ultralow Wear PTFE and Alumina Composites: It is All About Tribochemistry. *Tribol. Lett.* **2015**, *57*, 4.
(21) Harris, K. L.; Pitenis, A. A.; Sawyer, W. G.; Krick, B. A.; Blackman, G. S.; Kasprzak, D. J.; Junk, C. P. PTFE Tribology and the Role of Mechanochemistry in the Development of Protective Surface Films. *Macromolecules* **2015**, *48*, 3739−3745.
(22) Krick, B. A.; Ewin, J. J.; McCumiskey, E. J. Tribofilm Formation and Run-In Behavior in Ultra-Low-Wearing Polytetrafluoroethylene (PTFE) and Alumina Nanocomposites. *Tribol. Trans.* **2014**, *57*, 1058.
(23) Krick, B. A.; Pitenis, A. A.; Harris, K. L.; Junk, C. P.; Sawyer, W. G.; Brown, S. C.; Rosenfeld, H. D.; Kasprzak, D. J.; Johnson, R. S.; Chan, C. D.; Blackman, G. S. Ultralow wear fluoropolymer composites: Nanoscale functionality from microscale fillers. *Tribol. Int.* **2016**, *95*, 245.
(24) Ye, J.; Khare, H. S.; Burris, D. L. Transfer film evolution and its role in promoting ultra-low wear of a PTFE nanocomposite. *Wear* **2013**, *297*, 1095.
(25) Ye, J.; Burris, D. L.; Xie, T. A Review of Transfer Films and Their Role in Ultra-Low-Wear Sliding of Polymers. *Lubricants* **2016**, *4*, 4.
(26) Burris, D. L.; Zhao, S.; Duncan, R.; Lowitz, J.; Perry, S. S.; Schadler, L. S.; Sawyer, W. G. A route to wear resistant PTFE via trace loadings of functionalized nanofillers. *Wear* **2009**, *267*, 653.
(27) Van Meter, K. E.; Junk, C. P.; Campbell, K. L.; Babuska, T. F.; Krick, B. A. Ultralow Wear Self-Mated PTFE Composites. *Macromolecules* **2022**, *55*, 3924.
(28) Ye, J.; Khare, H. S.; Burris, D. L. Transfer film evolution and its role in promoting ultra-low wear of a PTFE nanocomposite. *Wear* **2013**, *297*, 1095−1102.
(29) Ye, J.; Khare, H. S.; Burris, D. L. Quantitative characterization of solid lubricant transfer film quality. *Wear* **2014**, *316*, 133−143.
(30) Ye, J.; Burris, D.; Xie, T. A Review of Transfer Films and Their Role in Ultra-Low-Wear Sliding of Polymers. *Lubricants* **2016**, *4*, 4.
(31) Callister, W. D.*Materials Science and Engineering: An Introduction*, 7th ed.; John Wiley & Sons: New York, 2007.
(32) Schmitz, T. L.; Action, J. E.; Burris, D. L.; Ziegert, J. C.; Sawyer, W. G. Wear-Rate Uncertainty Analysis. *J. Tribol.* **2004**, *126*, 802.
(33) Khare, H. S.; Moore, A. C.; Haidar, D. R.; Gong, L.; Ye, J.; Rabolt, J. F.; Burris, D. L. Interrelated Effects of Temperature and Environment on Wear and Tribochemistry of an Ultralow Wear PTFE Composite. *J. Phys. Chem. C* **2015**, *119*, 16518.
(34) Campbell, K. L.; Sidebottom, M. A.; Atkinson, C. C.; Babuska, T. F.; Kolanovic, C. A.; Boulden, B. J.; Junk, C. P.; Krick, B. A. Ultralow Wear PTFE-Based Polymer Composites-The Role of Water and Tribochemistry. *Macromolecules* **2019**, *52*, 5268−5277.
(35) Krick, B. A.; Ewin, J. J.; Blackman, G. S.; Junk, C. P.; Gregory Sawyer, W. Environmental dependence of ultra-low wear behavior of polytetrafluoroethylene (PTFE) and alumina composites suggests tribochemical mechanisms. *Tribol. Int.* **2012**, *51*, 42.
(36) Pitenis, A. A.; Ewin, J. J.; Harris, K. L.; Sawyer, W. G.; Krick, B. A. In Vacuo Tribological Behavior of Polytetrafluoroethylene (PTFE) and Alumina Nanocomposites: The Importance of Water for Ultralow Wear. *Tribol. Lett.* **2014**, *53*, 189.
(37) Pitenis, A. A.; Harris, K. L.; Junk, C. P.; Blackman, G. S.; Sawyer, W. G.; Krick, B. A. Ultralow Wear PTFE and Alumina Composites: It is All About Tribochemistry. *Tribol. Lett.* **2015**, *57*, 4.
(38) Campbell, K. L.; Sidebottom, M. A.; Atkinson, C.; Babuska, T. F.; Kolanovic, C. A.; Boulden, B. J.; Junk, C. P.; Krick, B. A. Ultralow Wear PTFE-Based Polymer Composites-The Role of Water and Tribochemistry. *Macromolecules* **2019**, *52*, 5268−5277.
(39) Sidebottom, M. A.; Atkinson, C. A.; Campbell, K. L.; Babuska, T. F.; Junk, C. P.; Burch, H. E.; Krick, B. A. Perfluoroalkoxy (PFA)-*α*-Alumina Composites: Effect of Environment on Tribological Performance. *Tribol. Lett.* **2019**, *68*, 14.
(40) Onodera, T.; Kawasaki, K.; Nakakawaji, T.; Higuchi, Y.; Ozawa, N.; Kurihara, K.; Kubo, M. Chemical reaction mechanism of polytetrafluoroethylene on aluminum surface under friction condition. *J. Phys. Chem. C* **2014**, *118*, 5390.
(41) Onodera, T.; Park, M.; Souma, K.; Ozawa, N.; Kubo, M. Transfer-film formation mechanism of polytetrafluoroethylene: A computational chemistry approach. *J. Phys. Chem. C* **2013**, *117*, 10464.
(42) Onodera, T.; Kawasaki, K.; Nakakawaji, T.; Higuchi, Y.; Ozawa, N.; Kurihara, K.; Kubo, M. Tribocatalytic Reaction of Polytetrafluoroethylene Sliding on an Aluminum Surface. *J. Phys. Chem. C* **2015**, *119*, 15954−15962.
(43) Harris, K. L.; Pitenis, A. A.; Sawyer, W. G.; Krick, B. A.; Blackman, G. S.; Kasprzak, D. J.; Junk, C. P. PTFE Tribology and the Role of Mechanochemistry in the Development of Protective Surface Films. *Macromolecules* **2015**, *48*, 3739−3745.

https://doi.org/10.1021/acsami.2c13644
ACS Appl. Mater. Interfaces 2022, 14, 54293−54303

(44) Bhargava, S.; Blanchet, T. A. Unusually effective nanofiller a contradiction of microfiller-specific Mechanisms of PTFE Composite Wear Resistance? *J. Tribol.* **2016**, *138*, 042001.
(45) Brunauer, S.; Emmett, P. H.; Teller, E. Adsorption of Gases in Multimolecular Layers. *J. Am. Chem. Soc.* **1938**, *60*, 309−319.
(46) Burris, D. L.; Sawyer, W. G. Addressing Practical Challenges of Low Friction Coefficient Measurements. *Tribol. Lett.* **2009**, *35*, 17−23.
(47) Sebastiani, M.; Johanns, K. E.; Herbert, E. G.; Pharr, G. M. Measurement of fracture toughness by nanoindentation methods: Recent advances and future challenges. *Curr. Opin. Solid State Mater. Sci.* **2015**, *19*, 324−333.
(48) Ghidelli, M.; Sebastiani, M.; Johanns, K. E.; Pharr, G. M. Effects of indenter angle on micro-scale fracture toughness measurement by pillar splitting. *J. Am. Ceram. Soc.* **2017**, *100*, 5731−5738.
(49) Muchtar, A.; Lim, L. C. Indentation fracture toughness of high purity submicron alumina. *Acta Mater.* **1998**, *46*, 1683−1690.
(50) Pavia, A.; Laurent, C.; Weibel, A.; Peigney, A.; Chevallier, G.; Estournès, C. Hardness and friction behavior of bulk CoAl2O4 and Co-Al2O3 composite layers formed during Spark Plasma Sintering of CoAl2O4 powders. *Ceram. Int.* **2012**, *38*, 5209−5217.

https://doi.org/10.1021/acsami.2c13644
ACS Appl. Mater. Interfaces 2022, 14, 54293−54303